

written in the explicit form only for a certain choice of coordinate axes. Given that the normal to the surface is parallel to axis z , we have

$$\widehat{V}_2 = \gamma_2(\hat{\sigma}_x \hat{p}_x - \hat{\sigma}_y \hat{p}_y), \quad (7)$$

with $\gamma_2 \neq 0$ being valid also for a symmetric quantum well. For two-dimensional planar systems, Hamiltonians V_1 and V_2 are unitarily equivalent, their spectra are identical and depend only on the moduli $|\gamma_1|$ and $|\gamma_2|$. These statements are invalid in the case of curved surfaces.

The Schrödinger equation including the spin-orbit interaction admits an exact analytical solution for the case of a hollow circular cylinder (nanotube). The energy eigenvalues turn out to be noninvariant with respect to a change in the sign of the spin-orbit interaction constant: they contain the products $\gamma_1 R$ and $\gamma_2 R$. This suggests a difference between the energy spectra of concave and convex systems (it should be recalled that in the model under consideration we are dealing with an oriented surface, i.e., directions \mathbf{n} and $-\mathbf{n}$ are physically nonequivalent).

In the experiment, the sign of γ_1 can manifest itself in the absorption of an electromagnetic wave, linearly polarized along the cylinder axis, by nanotube electrons. Depending on the senses of γ_1 and the curvature, the absorption maximum at the spin-flip transition is shifted to the right or to the left from the position corresponding to the planar structure of the same material. The contribution V_2 to the thermodynamic and optical characteristics of the system after summation over states are independent of the sign of γ_2 .

Taken together, the above considerations suggest the possibility, in principle, to distinguish between the contributions V_1 and V_2 when measuring one and the same response of the systems differing only in the sense of the curvature (e.g., GaAs/GaAlAs heterojunction) bent in such a way that electrons occur either on the internal or external surface of the cylinder.

5. Effect of spin-orbit interaction between two-dimensional electrons on the magnetization of nanotubes

The Schrödinger equation including spin-orbit coupling can be solved also in the case when a homogeneous magnetic field aligned parallel to the nanotube axis is applied to the system. Given a zero longitudinal momentum and a magnetic flux through the nanotube equal to a half-integer number of flux quanta, there is crossing of terms related to different spin projections. This peculiarity of the energy spectrum is responsible for the anomalies in the system's magnetization behavior.

In the absence of spin-orbit interaction, linear susceptibility corresponds to diamagnetism. If the spin-orbit coupling for a certain range of parameters of the problem is included, the sign of susceptibility may be changed (diapara-transition). For the same reason (term crossing), the magnetic susceptibility of the nanotube is characterized by marked dispersion in the low-frequency region (several orders of magnitude lower than the frequency of the electron rotational quantum $\hbar^2/2mR^2$).

We have also demonstrated that the incidence of an electromagnetic wave linearly polarized along the nanotube axis (with the external magnetic field oriented in the same direction) gives rise to a constant magnetic moment proportional to the wave intensity. This photoinduced magnetization is proportional to γ_1^2 (in the Rashba model), shows

resonant dependence on the wave frequency, and attains maximum at the spin-flip transition frequency.

The effect discussed in the present paper is akin to the photogalvanic one in that the preferred direction of the circular current that induces magnetic moment is given by the vector product $[\mathbf{B} \times \mathbf{n}]$, where the normal \mathbf{n} is directed along the cylinder radius. The second-order response to the electric field of the wave contains second and zero harmonics, the latter being responsible for constant magnetization.

References

1. Magarill L I, Romanov D A, Chaplik A V *Pis'ma Zh. Eksp. Teor. Fiz.* **64** 421 (1996) [*JETP Lett.* **64** 460 (1996)]; *Zh. Eksp. Teor. Fiz.* **110** 669 (1996) [*JETP* **83** 361 (1996)]; **113** 1411 (1998); *Superlattices Microstruct.* **23** 1227 (1998); *Physica B* **249–251** 377 (1998) [*JETP* **86** 771 (1998)]
2. Magarill L I, Chaplik A V *Zh. Eksp. Teor. Fiz.* **115** 1478 (1999) [*JETP* **88** 815 (1999)]; *Pis'ma Zh. Eksp. Teor. Fiz.* **68** 136 (1998) [*JETP Lett.* **68** 148 (1998)]; **70** 607 (1999) [**70** 615 (1999)]
3. Vedernikov A I, Chaplik A V *Zh. Eksp. Teor. Fiz.* **117** 449 (2000) [*JETP* **90** 397 (2000)]
4. Chaplik A V *Pis'ma Zh. Eksp. Teor. Fiz.* **62** 885 (1995) [*JETP Lett.* **62** 900 (1995)]; *Phys. Low-Dim. Struct.* (9/10) 131 (1999)

PACS numbers: 72.20 My, 73.40 Kp

DOI: 10.1070/PU2000v043n03ABEH000699

Tunneling measurements of the Coulomb pseudogap in a two-dimensional electron system in a quantizing magnetic field

É V Devyatov, A A Shashkin, V T Dolgoplov, V Hansen, M Halland

It is well known that the injection of a charge in the case of tunneling into a two-dimensional electron system placed in a quantizing magnetic field is highly sensitive to multiparticle effects. Tunneling may occur into the edge of a two-dimensional system (lateral tunneling) [1–3] and into its entire plane (vertical tunneling) [4–10]. It has been demonstrated in Refs [4, 5] that vertical tunneling is sensitive to both real spectral gaps at integer filling factors and the Coulomb pseudogap undergoing a shift concurrent with the Fermi level shift.

A survey of tunneling between identical highly mobile two-dimensional systems in the ultraquantum limit has revealed a pseudogap with an exponentially small tunneling density of states [6]. Since the experiments in [4–6] have been performed on samples of different quality and in different magnetic field limits, it long remained unclear whether the gaps observed were of similar or different nature. A recent study [7] has demonstrated that all previously obtained results may be reproduced using one sample. Therefore, it is inferred that Refs [4–6] describe the same pseudogap. Ref. [8], in which the method of an earlier study [6] was employed, reports surprising evidence that the width of the pseudogap at a filling factor $\nu = 1/2$ can be proportional to the magnetic field.

An enhancement of the pseudogap in the vicinity of $\nu = 1$ accompanied by the appearance of a double-humped structure in the tunneling resistance has been documented in experiments on tunneling from a three-dimensional electron system into a highly mobile two-dimensional electron gas [9].

This finding was recently confirmed in a study on tunnel current relaxation [10], which also gave evidence of two significantly different relaxation times near $\nu = 1$.

Numerous theoretical works predicted the existence of a pseudogap in metallic and dielectric phases of two-dimensional electron systems. In the case of a two-dimensional metal with a slight disorder, the electron–electron interaction leads to logarithmic corrections which tend to decrease the density of states at the Fermi level [13]. At the same time, the tunneling density of states at the Fermi level ε_F in the dielectric phase vanishes according to the law

$$D = \frac{2\kappa^2}{\pi e^4} |\varepsilon - \varepsilon_F|,$$

where κ denotes the dielectric permeability, ε is the energy, and e is the electron charge [14].

The presence of a Coulomb pseudogap with an exponentially small density of states near the Fermi level ε_F has also been predicted for the metallic phase in a quantizing magnetic field [15–18]. A similar result was obtained for tunneling into the Wigner crystal [19] and into the dielectric state of a slightly disordered two-dimensional system at large filling factors [20]. According to Refs [15, 16, 19], the pseudogap width must be determined by the average distance between electrons. In the dielectric phase of a highly disordered system [21], one should anticipate the development of a linear-in-energy pseudogap of the form

$$D(\varepsilon) = D_F + \alpha |\varepsilon - \varepsilon_F|, \quad (1)$$

where the coefficient α differs from $\alpha_0 = 2\kappa^2/\pi e^4$ predicted in Ref. [14].

The results of the above theoretical studies are in qualitative agreement with experimental findings. The following discrepancies between the theory and experiment should however be emphasized: (1) there is a disproportion between the gap size and the average interelectron distance [8]; (2) experiments reveal a decrease in the coefficient α with increasing magnetic field [7]; (3) the theory does not explain the pseudogap behavior near the $\nu = 1$ filling [9, 10].

The aim of the present work was a comprehensive investigation into the tunneling from a three-dimensional system into a highly mobile two-dimensional electron system at filling factors $\nu \leq 1$. The experiments were made using (Al,Ga)As/GaAs heterostructures with a metallic gate at the crystal surface; they also contained a 20-nm highly doped silicon layer ($4 \times 10^{18} \text{ cm}^{-3}$) buried in GaAs. This layer possessed the properties of a ‘dirty’ three-dimensional conductor.

The sample structure and the computed behavior of the bottom of the conduction band are shown in Fig. 1. Four samples were prepared using two wafers grown in two different molecular-beam epitaxy chambers. The short-period GaAs/AlAs superlattice served as a blocking barrier between the two-dimensional electron layer and the gate, while the wide but shallow tunnel barriers were created by the weak residual p doping in GaAs.

The electron density was specified by a constant voltage V_g applied between the gate and the three-dimensional contact. The distances shown in Fig. 1 were $x_g^0 = 142 \text{ nm}$, $x_w^0 = 100 \text{ nm}$, and $x_g = 142.4 \text{ nm}$, $x_w = 100 \text{ nm}$ for structures *A* and *B* respectively. The gate area was $8700 \mu\text{m}^2$ for sample *A1*, $800 \mu\text{m}^2$ for samples *A2* and *A3*, and $3300 \mu\text{m}^2$ for sample *B*.

By modulating the gate voltage and measuring the imaginary and real current components, we obtained infor-

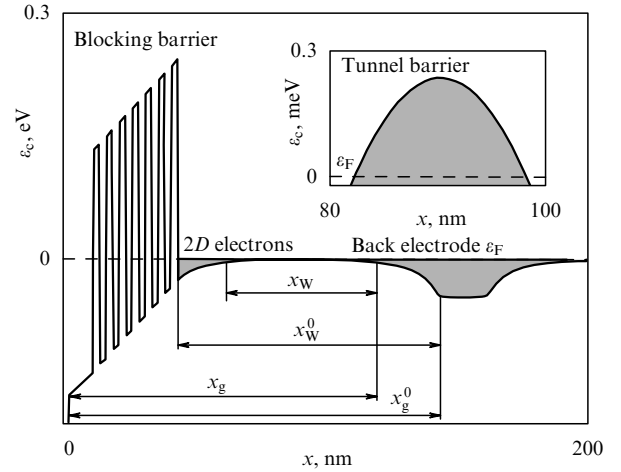


Figure 1. Energy of the bottom of the conduction band ε_c as a function of the distance x at $V_g = 0.8$. The tunnel barrier is depicted in the inset.

mation about the thermodynamic density of states and tunneling resistance. The following equation was used to calculate these parameters [5, 9]:

$$\frac{I}{V} = \omega \left(\frac{\omega\tau + i}{1 + \omega^2\tau^2} (C_{\text{low}} - C_{\text{high}}) + iC_{\text{high}} \right). \quad (2)$$

Here, $\omega/2\pi$ is the frequency of the alternating current, and C_{low} and C_{high} are the low- and high-frequency limits, respectively, of the device capacitance being measured.

The relaxation time τ in Eqn (2) was

$$\tau = R_{\text{tun}} (C_{\text{low}} - C_{\text{high}}) \left(\frac{x_g}{x_w} \right)^2, \quad (3)$$

$$R_{\text{tun}} = \frac{\tau_{\text{tun}}}{AD_S e^2} = \frac{\rho_{\text{tun}}}{A},$$

where R_{tun} is the tunneling resistance, τ_{tun}^{-1} is the frequency of attempts, D_S is the single-particle density of states, and the distances x_g , x_w substitute for x_g^0 , x_w^0 in accordance with the real distribution of electron density in the x direction.

In the low-frequency limit, nonlinear tunnel current–voltage characteristics were deduced from the measured values of $\text{Re } I$ and $\text{Im } I$ using the relations

$$V_{\text{tun}} = \frac{C_{\text{low}} \text{Re } I}{\omega (C_{\text{low}} - C_{\text{high}})^2} \left(\frac{x_w}{x_g} \right)^2, \quad I_{\text{tun}} = \text{Im } I. \quad (4)$$

Here, the quantity eV_{tun} is the difference of the electrochemical potentials between the two-dimensional electron layer and the three-dimensional contact. In the analysis of nonlinear current–voltage characteristics, it was assumed that the measured signal corresponded to the first Fourier harmonic of the alternating current.

Typical experimental curves in the low-frequency limit are presented in Fig. 2. The imaginary component of the current with the minima at integer and fractional filling factors is known to carry information about the thermodynamic density of states [12, 22]. The real component of the current contains a double-humped structure at $\nu \approx 1$ [9, 10] and peaks at $\nu = 1/3$ and $\nu = 2/3$, along with a signal showing weak dependence on the filling factor described earlier in Refs [4–8]. In principle, similar structures can arise during electron transfer along a two-dimensional layer due to the tunnel current inhomogeneity.

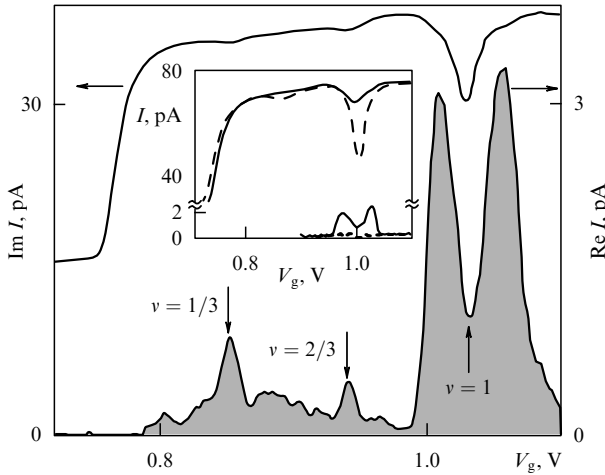


Figure 2. Imaginary and real current components plotted as functions of the gate voltage in a 14-T magnetic field for sample A1; $T = 30$ mK, $V = 4.2$ mV, $\omega/2\pi = 73$ Hz. In the inset: experimental records in 6.9-T (dashed line) and 13.7-T (solid line) magnetic fields for sample B; $T = 60$ mK, $V = 2.1$ mV, $\omega/2\pi = 920$ G.

In our case, the structures observed at $\nu = 1$ are not related to lateral transport, because (1) analogous structures were lacking at the same temperature at filling factor $\nu = 2$ (notwithstanding a significantly lower dissipative conductivity at this value of the filling factor); (2) the frequency, temperature and magnetic-field dependences of the active current component and its current–voltage characteristics discussed below are incompatible with the assumption of lateral transport; and (3) similar features were observed near $\nu = 1$ in an afore-mentioned study (see Ref. [10]), although these experiments were made on samples with a differently shaped tunnel barrier.

The real component of the current had the shape resembling that in Fig. 2, with two maxima at $\nu \approx 1$ in the minimum magnetic field in which the corresponding structure was still discernible (in a 8-T field for improved samples from structure A and in a 11-T field for a sample from wafer B).

The frequency dependence of the current at the maximum and minimum of tunneling resistance at $\nu \approx 1$ is illustrated by Fig. 3. Eqn (2) fairly well describes experimental findings provided the quantity C_{high} is replaced by the fitting parameter $C_0 > C_{\text{high}}$. The necessity of introduction of the fitting parameter C_0 suggests the existence of at least two significantly different relaxation times.

The relation $\beta = (C_{\text{low}} - C_0)/(C_{\text{low}} - C_{\text{high}})$ gives the fraction of tunneling processes with the highest tunneling resistance ρ_{tun} (and maximum relaxation time τ) or the ‘fraction of the area’ corresponding to such processes. In the low-frequency limit under discussion, the tunnel current corresponding to a large relaxation time is proportional to β . In other words, I_{tun} in (4) should be replaced by $I_{\text{tun}} = \beta \text{Im } I$, whereas expressions for V_{tun} and R_{tun} in (3) and (4) remain unaltered.

The solid lines in Fig. 3 correspond to $\beta \approx 1$ and $\beta \approx 0.6$ for the tunneling-resistance maximum and minimum, respectively. The double-humped curve also holds for R_{tun} ; that is, the division of $\text{Re } I$ by $\beta(C_{\text{low}} - C_{\text{high}})^2$ leaves the tunneling resistance minimum, having a depth of about 30%, at point $\nu = 1$.

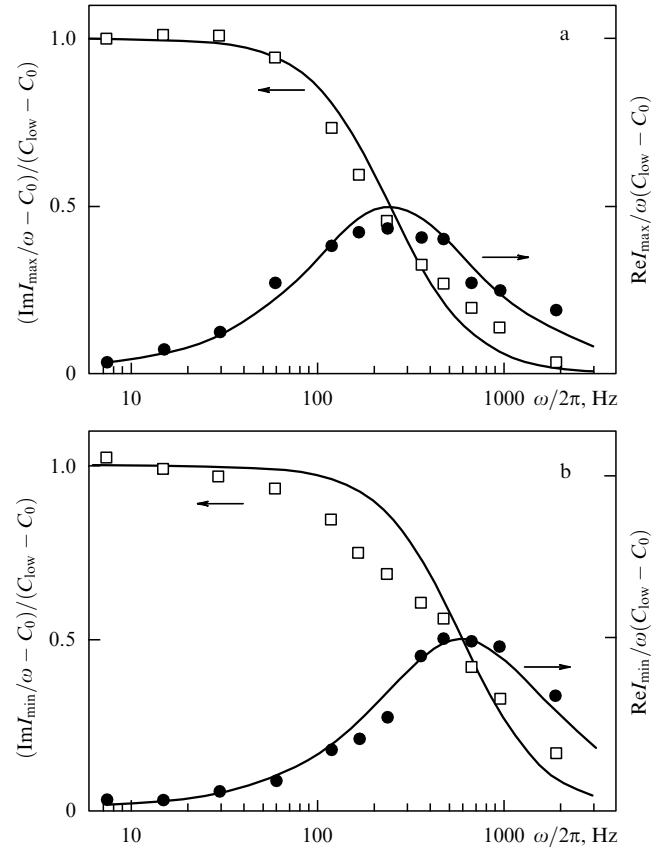


Figure 3. Frequency dependence of the imaginary and real current components at (a) maximum and (b) minimum tunneling resistances R_{tun} for sample A1, $T = 30$ mK, $B = 10$ T. Solid lines result from a fit using Eqn (2) and fitting parameters τ and C_0 .

An example of a current–voltage characteristic is presented in Fig. 4. Experimentally measured dependences are roughly parabolic at $eV_{\text{tun}} > k_B T$ and linear at $eV_{\text{tun}} < k_B T$. The parabolic dependence corresponds to a linear pseudogap. In order to describe the experimental results, we calculated the first Fourier harmonic of the voltage on the nonlinear element $V_{\text{tun}}(I_{\text{tun}})$ given by the condition

$$I_{\text{tun}} = \gamma \int_{-\infty}^{\infty} D_m D(\varepsilon) [f(\varepsilon - eV_{\text{tun}}, T) - f(\varepsilon, T)] d\varepsilon, \quad (5)$$

where γ denotes an unknown coefficient; function $D(\varepsilon)$ is given by Eqn (1) with $D_F = 0$; and $f(\varepsilon, T)$ is the Fermi–Dirac distribution. The density of states in the injecting electrode is assumed to be independent of the magnetic field. It follows from Fig. 4 that the computed curve fairly well describes experimental findings even if using a single fitting parameter $\alpha\gamma D_m$.

Assuming that the quantities γ and D_m remain unaltered for a given sample, it is possible to determine the magnetic-field and temperature dependences of the coefficient α from the current–voltage characteristics. It turns out that α tends to saturate in strong magnetic fields and at low temperatures; conversely, the pseudogap vanishes in the opposite limit.

We also measured current–voltage characteristics in strong magnetic fields for filling factors $\nu = 1/2$ and $\nu = 2/3$. At $\nu = 1/2$, the experimental current–voltage curve turned out to be nearly parabolic, in agreement with

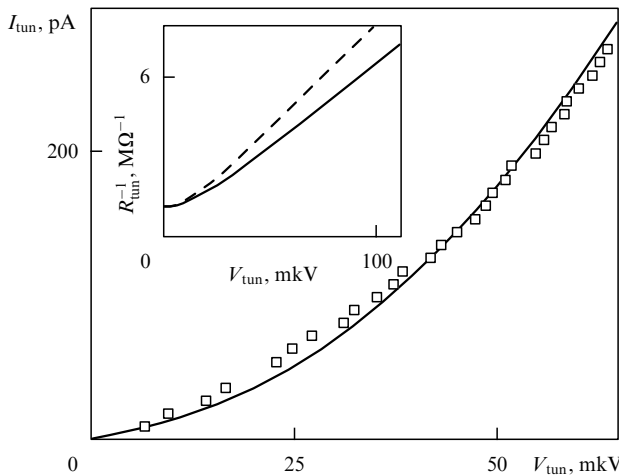


Figure 4. Comparison of measured and computed [Eqn (5)] current–voltage characteristics in the R_{tun} maximum at $\nu \approx 1$ for sample B; $T = 60$ mK, $B = 13$ T. The inset shows the fitting curve for V_{tun} , R_{tun}^{-1} before (dashed line) and after (solid line) computation of the first Fourier harmonic.

the results of earlier experiments [7]. The current–voltage characteristics for the filling factor $\nu = 2/3$ were close to linear ones even at $eV_{\text{tun}} > k_B T$, although the linear range shrank with increasing temperature.

To conclude, we have confirmed the existence of a linear-in-energy pseudogap over a wide range of filling factors at $\nu < 1$ (outside the tunneling-resistance peaks at $\nu = 1/3$ and $\nu = 2/3$) and demonstrated that the linear energy dependence also holds for a double-humped structure near $\nu = 1$. It follows from the analysis of current–voltage characteristics that the coefficient α peaks at $\nu = 1$. By comparing the positions of the peaks of the real current component near $\nu = 1$ and metal–insulator transition points in samples of similar quality [23], the filling factors corresponding to the peaks were found to coincide with the filling factors at the transition points. In principle, the available theoretical models allow one to describe a decrease of the coefficient α associated with a deviation of the filling factor from $\nu = 1$.

According to Refs [17, 18], tunneling into the metallic phase leads to the development of a pseudogap related to the finite time of charge dissipation in the plane. The higher the conductance in the plane, the narrower the gap. The shape of the gap in the metallic phase is given by the expression

$$D(\varepsilon) = D_{\text{th}} \exp\left(-\ln^2 \frac{e^4}{\alpha^2 K |\varepsilon - \varepsilon_F|}\right). \quad (6)$$

Here, D_{th} is the thermodynamic density of states and K is the diffusion coefficient [18, 24]. According to [24], dependence (6) in the energy interval $|\varepsilon - \varepsilon_F| < U_c = e^2/\alpha\xi$ (ξ is the mean dimension of the conducting cluster) must be replaced by $\alpha|\varepsilon - \varepsilon_F|$, where $\alpha = D(\varepsilon_F + U_c)/U_c$. It has been shown experimentally that the coefficient α increases as $\nu \rightarrow 1$, because the correlation length ξ decreases with penetration deeper into the dielectric phase.

This work was supported by the Russian Foundation for Basic Research (project 97-02-16829); the Program “Physics of Solid-State Nanostructures” (project 97-1024) and Program “Statistical Physics” of the Russian Ministry of Science and Technology; and Program “Physics of Nanostructured Solids” (Deutsche Forschungsgemeinschaft, Germany).

References

1. Chang A M, Pfeiffer L N, West K W *Phys. Rev. Lett.* **77** 2538 (1996)
2. Grayson M et al. *Phys. Rev. Lett.* **80** 1062 (1998)
3. Shashkin A A et al. *Pis'ma Zh. Eksp. Teor. Fiz.* **69** 561 (1999) [*JETP Lett.* **69** 603 (1999)]
4. Ashoori R C et al. *Phys. Rev. Lett.* **64** 681 (1990)
5. Ashoori R C et al. *Phys. Rev. B* **48** 4616 (1993)
6. Eisenstein J P, Pfeiffer L N, West K W *Phys. Rev. Lett.* **69** 3804 (1992); **74** 1419 (1995)
7. Chan H B et al. *Phys. Rev. Lett.* **79** 2867 (1997)
8. Brown K M et al. *Phys. Rev. B* **50** 15465 (1994)
9. Dolgoplov V T et al. *Phys. Rev. B* **51** 7958 (1995)
10. Chan H B et al., cond-mat/9905371
11. Eisenstein J P, Pfeiffer L N, West K W *Phys. Rev. B* **50** 1760 (1994)
12. Dolgoplov V T et al. *Phys. Rev. Lett.* **79** 729 (1997)
13. Altshuler B L, Aronov A G, Lee P A *Phys. Rev. Lett.* **44** 1288 (1980)
14. Efros A L, Shklovskii B I, in *Electron–Electron Interaction in Disordered Systems* (Eds A L Efros, M Pollak) (Amsterdam: North-Holland, 1985)
15. Efros A L *Phys. Rev. Lett.* **68** 2208 (1992)
16. Hatsugai Y, Bares P -A, Wen X G *Phys. Rev. Lett.* **71** 424 (1993)
17. He S, Platzman P M, Halperin B I *Phys. Rev. Lett.* **71** 777 (1993)
18. Levitov L S, Shytov A V *Pis'ma Zh. Eksp. Teor. Fiz.* **66** 200 (1997) [*JETP Lett.* **66** 214 (1997)]
19. Johansson P, Kinaret J M *Phys. Rev. Lett.* **71** 1435 (1993)
20. Aleiner I L, Baranger H U, Glazman L I *Phys. Rev. Lett.* **74** 3435 (1995)
21. Yang S -R E, MacDonald A H *Phys. Rev. Lett.* **70** 4119 (1993)
22. Dolgoplov V T et al. *Phys. Low-Dim. Struct.* (6) 1 (1996)
23. Shashkin A A et al. *Phys. Rev. Lett.* **73** 3141 (1994)
24. Polyakov D G, Samokhin K V *Phys. Rev. Lett.* **80** 1509 (1998)

PACS numbers: 75.60.-d, 75.70.-k
DOI: 10.1070/PU2000v043n03ABEH000700

Collective effects in artificial two-dimensional lattices of ferromagnetic nanoparticles

S A Gusev, Yu N Nozdrin, M V Sapozhnikov, A A Fraerman

Many studies of zero-dimensional nanostructures are focused on the creation and investigation of ferromagnetic nanoparticles. On the one hand, interest in these particles is due to the possibility of their practical application, in the first place for the development of recording media that can ensure super-high (over 10^{10} bit cm^{-2}) data storage densities [1]. On the other hand, studies of ferromagnetic nanoparticles bring about new knowledge of the properties of magnetic materials at supersmall scales.

We believe that the collective behavior of ferromagnetic nanoparticles during their interaction is one of the most interesting aspects of the problem in question. Stray fields induced by individual particles constitute the fundamental cause of this interaction. In the case of a single-domain particle, the major contribution comes from dipole interaction. Elucidation of this mechanism has important practical implications, because it may be useful for the assessment of data density limits.

Creation of systems of interacting ferromagnetic nanoparticles opens good prospects for the control of magnetic properties. Indeed, if we mentally substitute single-domain supermagnetic particles for magnetic atoms, it would be possible, by virtue of their dipole interaction, to effect a